ARTICLES
PUBLISHED ONLINE: 2 OCTOBER 2017 | DOI: 10.1038/NNANO.2017.207
nature nanotechnology

Inner- and outer-wall sorting of double-walled carbon nanotubes

Han Li[1]*, Georgy Gordeev[2], Sören Wasserroth[2], Venkata Sai Kiran Chakravadhanula[1,3], Shyam Kumar Chethala Neelakandhan[1,4], Frank Hennrich[1], Ado Jorio[5], Stephanie Reich[2], Ralph Krupke[1,4] and Benjamin Scott Flavel[1,4]*

Double-walled carbon nanotubes (DWCNTs) consist of two coaxially aligned single-walled carbon nanotubes (SWCNTs), and previous sorting methods only achieved outer-wall electronic-type selectivity. Here, a separation technique capable of sorting DWCNTs by semiconducting (S) or metallic (M) inner- and outer-wall electronic type is presented. Electronic coupling between the inner and outer wall is used to alter the surfactant coating around each of the DWCNT types, and aqueous gel permeation is used to separate them. Aqueous methods are used to remove SWCNT species from the raw material and prepare enriched DWCNT fractions. The enriched DWCNT fractions are then transferred into either chlorobenzene or toluene using the copolymer PFO-BPy to yield the four inner@outer combinations of M@M, M@S, S@M and S@S. The high purity of the resulting fractions is verified by absorption measurements, transmission electron microscopy, atomic force microscopy, resonance Raman mapping and high-density field-effect transistor devices.

Double-walled carbon nanotubes (DWCNTs) are a unique nanostructure consisting of two concentric single-walled carbon nanotubes (SWCNTs) and have four different electronic types. These are broadly defined by the constituent inner and outer walls, which can be metallic (M) or semiconducting (S), thus giving four possible electronic combinations—M@M, S@M, M@S and S@S—where the notation is inner@outer wall[1]. Electronic and physical coupling between the two walls has been shown theoretically[2] and experimentally[3] to lead to new properties not observed in SWCNTs. Therefore, DWCNTs must be considered as a new and separate nanostructure[4] rather than the combination of two SWCNTs, and these new properties are expected to open exciting avenues for carbon science in the future, such as superconductivity in M@M DWCNTs[5], wavefunction mixing within two commensurate semiconducting walls to afford a DWCNT with overall metallic properties[6], and the emergence of new and/or shifted optical modes[7] due to pressure exerted on the inner wall by the outer wall. DWCNTs are also the simplest form of multi-walled carbon nanotube (MWCNT) and provide a test system to study the physics of two interacting carbon walls, for example by probing electron or exciton transfer or by measuring the shear force between the two walls in a 'telescoping' experiment. In fact, superlubricity has already been observed in DWCNTs[8] and they have been proposed to be candidates for the development of all carbon actuators. DWCNTs have also been idealized in the development of carbon-nanotube field-effect transistors (CNT–FETs), either for chemical and biological sensors where the outer wall acts as a scaffold for modification with receptor molecules[9] or, alternatively, where the outer wall acts to shield the inner wall from the external environment[10], avoiding substrate-induced doping effects.

Initially, the study of DWCNTs was made difficult owing to the inability to grow pure DWCNT samples, and research efforts were directed towards removing the SWCNT and MWCNT impurities from the as-grown raw material[1]. As methods to obtain pure DWCNT fractions improved, the research focus turned to electronic type separation, and in the best examples both type selection and the removal of impurities were achieved in a single approach. For example, Green *et al.*[11] used density gradient ultracentrifugation to separate SWCNTs from DWCNTs based on their buoyant density, and later used co-surfactant mixtures of sodium dodecyl sulfate (SDS) and sodium cholate (SC) to separate DWCNTs with defined outer-wall electronic types[10]. Similarly, Moore *et al.*[12] used co-surfactant mixtures of SDS and SC to elute three distinct bands containing (in order of elution) X@M, X@S and SWCNTs from a Sephacryl gel column, where X indicates an unknown or unsorted inner wall. Most recently, Streit *et al.*[13] have shown that DWCNTs can be sorted by diameter using the aqueous two-phase extraction method, but, similar to Green and Moore, they were only able to achieve outer-wall electronic-type selectivity. Separation of DWCNTs with selectivity for both the inner and outer wall has remained a challenge thus far.

In all previous approaches, the structure of the surfactant layer, which is essentially responsible for separation, was entirely defined by the outer-wall electronic type, and the inner wall appeared to be completely decoupled from the surrounding surfactant solution. However, electronic coupling between the two walls of a DWCNT and the well-known sensitivity of separation methods to electronic type tend to suggest that it must be possible to modulate the surrounding surfactant shell based on the inner-wall type. In the current work, optimized conditions are used, and it is shown that electronic coupling between the walls can be used to modulate the surrounding surfactant shell. The X@M and X@S fractions from ref. 12 were resolved into their subcomponents, M@M/S@M and M@S/S@S, respectively, using the approach shown schematically in Fig. 1a. A different surfactant coating was predicted to be obtained around each of the four different types of DWCNT, and a single gel column was used to separate them. Gel permeation chromatography was used to obtain a pre-selection (indicated by

[1]Institute of Nanotechnology, Karlsruhe Institute of Technology, 76021 Karlsruhe, Germany. [2]Department of Physics, Freie Universität Berlin, 14195 Berlin, Germany. [3]Helmholtz Institute Ulm Electrochemical Energy Storage, 89081 Ulm, Germany. [4]Institute of Materials Science, Technische Universität Darmstadt, 64287 Darmstadt, Germany. [5]Department of Physics, Federal University of Minas Gerais, Belo Horizonte, Brazil. *e-mail: han.li@kit.edu; benjamin.flavel@kit.edu

© 2017 Macmillan Publishers Limited, part of Springer Nature. All rights reserved.

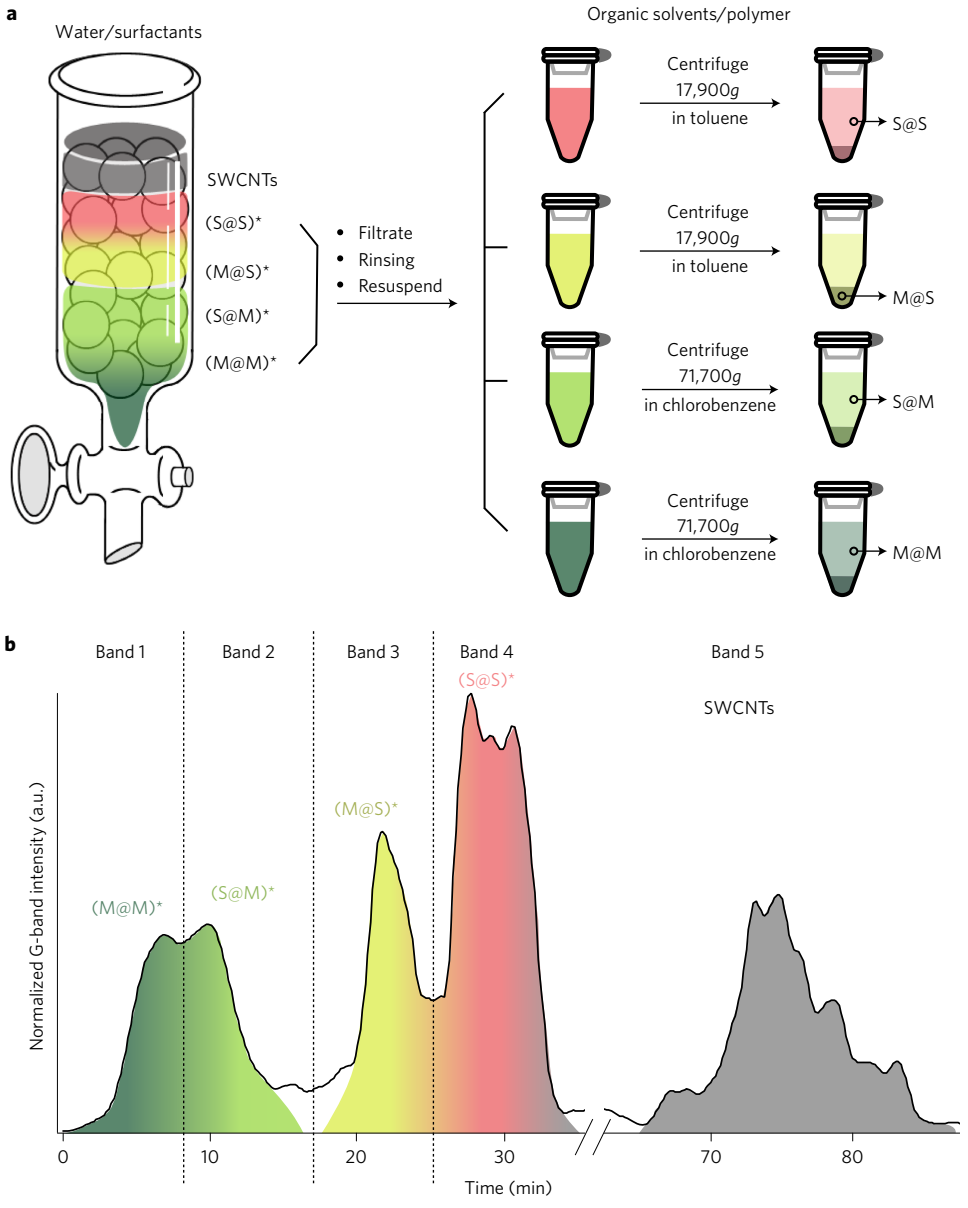

Figure 1 | Separation of DWCNTs via gel permeation. a, Surfactant-suspended DWCNTs are separated by gel permeation chromatography into five fractions: the four different types of DWCNT (indicated by an asterisk) and SWCNTs. Subsequently, the DWCNT fractions are transferred into an organic solvent with polymer wrapping to yield purified fractions of (M@M), (S@M), (M@S) and (S@S). **b**, Elution profile obtained during gel permeation chromatography by monitoring the normalized G-band Raman mode intensity at 785 nm laser excitation.

an asterisk) of the four different types of DWCNT, and these were then purified further by exchange to organic solvent with the aid of the co-polymer poly[(9,9-dioctylfluorenyl-2,7-diyl)-alt-co-(6,6′-{2,2′-bipyridine})] (PFO–BPy). Aqueous separation, organic purification and their role in obtaining the four different types of DWCNT are discussed in the following sections.

Separation by gel permeation

Similar to the work of Moore *et al.*[12], a co-surfactant mixture of SC and SDS was used for separation. However, in the current work, 1 mM NaOH was added to the nanotube suspension, the gel column and the SDS eluent. In Fig. 1b, a process Raman analyser is used to follow nanotube elution by monitoring the integrated G-band intensity versus time. It can be seen that the addition of NaOH resulted in five elution bands: four unadsorbed moving bands containing DWCNTs (0–30 min) and one adsorbed stationary band containing SWCNTs (~70–80 min). Additional process Raman elugrams for 0 and 4 mM NaOH are provided in Supplementary Fig. 1a, and absorption spectra of sequential 2 ml fractions using 0, 1 and 4 mM NaOH are shown in Supplementary Fig. 1b–d. The addition of NaOH has clearly altered the interaction of the nanotubes with the gel column and the mechanism behind this is explained in detail in the Supplementary Information (Supplementary Fig. 2). At this point it suffices to state that the addition of NaOH has increased the interaction strength of the nanotubes with the gel and this leads to almost complete adsorption of the SWCNT species to the gel and separation of the DWCNTs.

The addition of 1 mM NaOH was found to afford the best DWCNT separation, and clear changes in the spectral shape between fractions can be seen in Supplementary Fig. 1c. The spectra of DWCNTs are discussed here using a slightly modified notation taken from ref. 13. The optical transitions of a DWCNT are identified by E_{ii}^{wall}, where E represents the electronic type (S for semiconducting and M for metallic), ii refers to a specific

© 2017 Macmillan Publishers Limited, part of Springer Nature. All rights reserved.

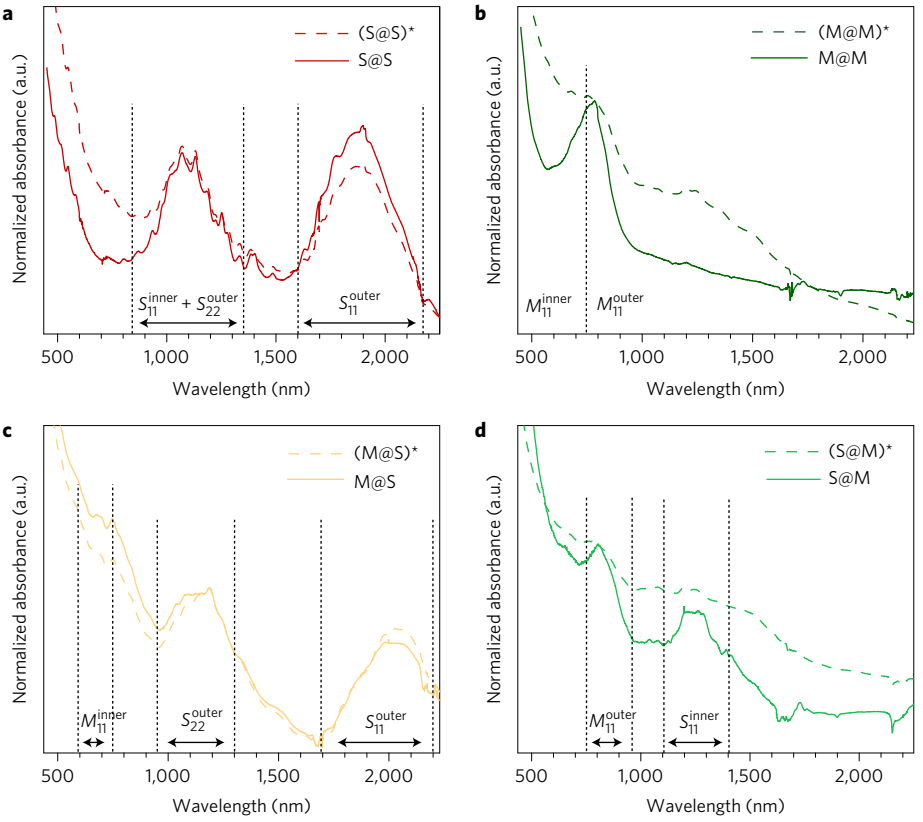

Figure 2 | Absorption spectra of the four different types of DWCNT. Spectra are shown before (dashed line) and after (solid line) polymer purification. **a**, (S@S)* and S@S. **b**, (M@M)* and M@M. **c**, (M@S)* and M@S. **d**, (S@M)* and S@M. To allow for comparison, spectra are normalized to 1 at 1,190 nm in **a**,**c** and at 800 nm in **b**,**d**.

transition and 'wall' refers to the inner or outer wall. For example, the first four fractions in Supplementary Fig. 1c assigned to band 1 of the elution profile in Fig. 1b show peaks between 750 and 950 nm that are indicative of the metallic M_{11} transitions of large-diameter (1.6–2.1 nm, from Hároz *et al.*[14]) nanotubes and can be written as M_{11}^{outer}. Similarly, the same fractions show peaks located between 600 and 700 nm, which are indicative of the metallic M_{11} transitions of small-diameter (0.9–1.3 nm) nanotubes and can be written as M_{11}^{inner}. For fractions 5–8 (band 2), the peak assigned to M_{11}^{outer} remains, but new peaks between 1,000 and 1,300 nm emerge, and are assigned to small-diameter (0.7–1.1 nm) (ref. 15) semiconducting nanotubes and labelled as S_{11}^{inner}. Fractions 9–11 (band 3) look very similar to band 2, except for a reduction in the broad peak centred around 750–900 nm that was assigned to M_{11}^{outer}, while the small peaks between 600 and 700 nm assigned to $M_{11}^{inner}$are maintained. In contrast, fractions 12–17 (band 4) are markedly different. In band 4, both M_{11}^{inner} and M_{11}^{outer} are absent and a broad peak between 900 and 1,350 nm, assigned to S_{11}^{inner} and S_{22}^{outer}, emerges. Based on this assignment, bands 1–4 each contain a different type of DWCNT and are labelled (M@M)*, (S@M)*, (M@S)* and (S@S)*, respectively. The final fractions 18–20 (band 5) contain sharp peaks between 1,000 and 1,300 nm and were assigned to small-diameter SWCNTs[16]. To assist comparison, all of the fractions assigned to an elution band were combined and the spectra are shown in Supplementary Fig. 3. Due to the large diameter of the outer wall (up to ~2 nm), with an expected S_{11}^{outer} of ~ 2,000 nm and overlapping S_{11}^{inner} and S_{22}^{outer} peaks, it is difficult to be certain of the validity of this assignment. The strong absorption of light at 1,500 and 1,900 nm for water and D_2O, respectively, only confounds this problem. This is especially true for samples (S@M)* and (M@S)*, which are spectrally similar, and where peaks assigned to S_{11}^{inner} or S_{22}^{outer} could also be S_{22}^{outer} or S_{11}^{inner} or indeed a combination of both. To correctly characterize DWCNTs in this diameter range it is important to measure above 2,000 nm and correlate pairs of first- and second-order optical transitions for the different wall types.

Purification by polymer wrapping

To enable measurement of the complete absorption spectra, the four types of DWCNT were filtered, washed, dried and resuspended in organic solvent with PFO–BPy, as shown in Fig. 1a. PFO–BPy was chosen due to its high semiconducting selectivity (purity > 99%, ref. 17) while remaining non-specific to (*n*,*m*) species in the large-diameter range[17]. Both (S@S)* and (M@S)* were redispersed in toluene. In the case of (S@S)*, the supernatant was collected after centrifugation and assigned S@S for further characterization. Alternatively, for (M@S)* the supernatant was discarded, the pellet collected and the process repeated until the ratio between the peaks assigned to M_{11}^{inner} and S_{22}^{outer} ceased to increase. The resultant sample was labelled M@S for further characterization. Figure 2 shows the absorption spectra of (S@S)* and S@S (Fig. 2a) and (M@S)* and M@S (Fig. 2c). Consideration of either (S@S)* or (M@S)* before centrifugation (dashed line) verified the initial spectral assignment made in water. The peak assigned to S_{22}^{outer} in the (M@S)* case has a corresponding S_{11}^{outer} at 2,050 nm, and in the (S@S)* case a matching S_{11}^{outer} can be found at 1,880 nm. The position of these two S_{11}^{outer} peaks suggest that the S@S DWCNTs are slightly smaller (~0.2 nm) in diameter than their M@S counterparts. Following centrifugation (solid line), the change in spectral shape closely matches what is expected for use of a polymer with high semiconducting selectivity[18]. The intensity of M_{11}^{inner} peaks at 600–700 nm is significantly decreased in the S@S sample by collecting the supernatant and significantly increased by collecting the pellet for M@S.

© 2017 Macmillan Publishers Limited, part of Springer Nature. All rights reserved.

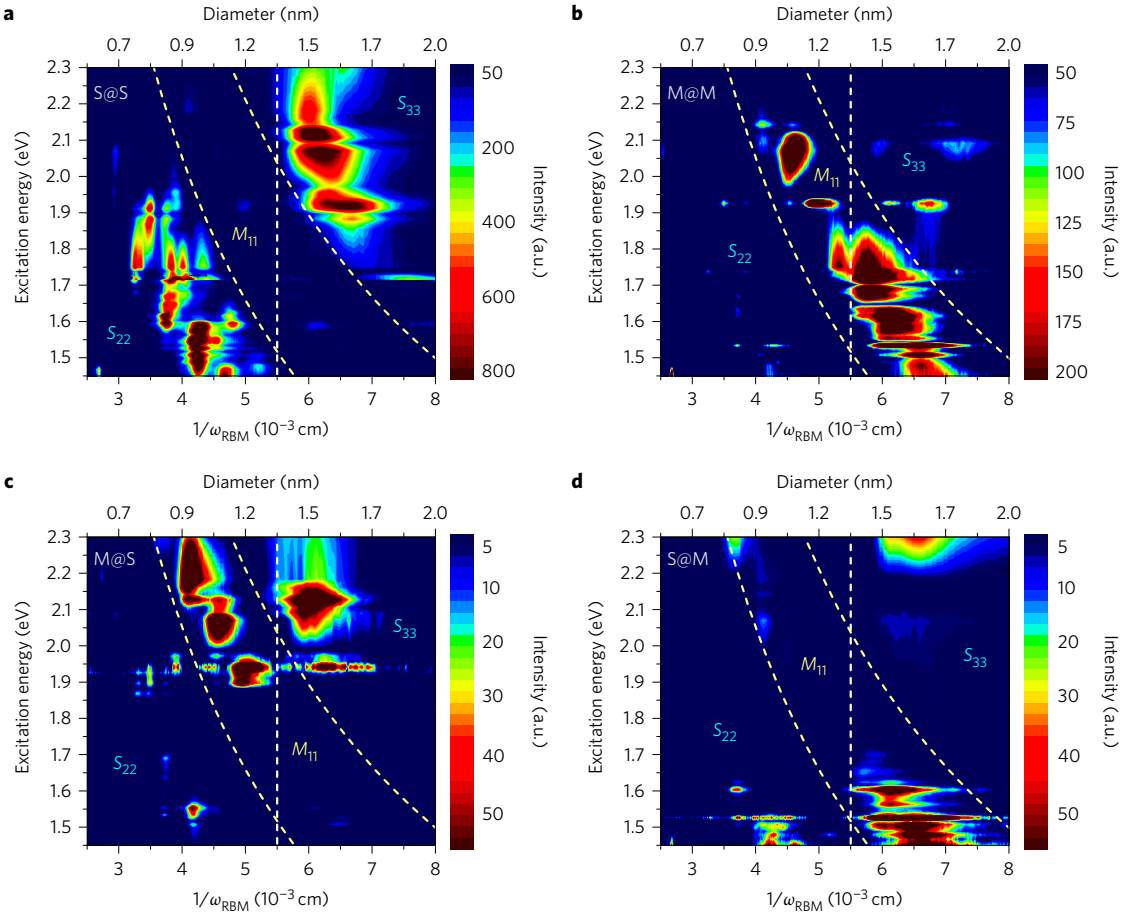

Figure 3 | Radial breathing mode resonance Raman maps. a, S@S. **b**, M@M. **c**, M@S. **d**, S@M. The two curved dashed lines divide the energy ranges where the resonance of semiconducting (S_{22})-metallic (M_{11})-semiconducting (S_{33}) take place in single-walled nanotubes[21,23]. Although the resonance energies and Raman cross-section vary from SWCNTs to DWCNTs[24,28], the overall trend does not change. To the right of the vertical dashed line appearing in the maps near $d_t = 1.3$ nm, the RBM signals come mostly from outer tubes (larger diameters), while to the left of this line, the RBM signals come mostly from inner tubes (small diameters).

For the metallic outer-wall species, electronic separation occurs exclusively in aqueous solution with the Sephacryl gel. However, (S@M)* and (M@M)* were redispersed in organic solvent to assist characterization. By using chlorobenzene as a solvent it was possible to collect the supernatant in both the (M@M)* and (S@M)* cases, and the fractions were labelled M@M and S@M. Figure 2 presents absorption spectra for (M@M)* and M@M (Fig. 2b) and (S@M)* and S@M (Fig. 2d). Despite the lack of electronic selectivity in chlorobenzene, PFO–BPy wrapping still improved the quality of both fractions after centrifugation (solid line), albeit for a different reason than for the semiconducting outer-wall species. In Fig. 2b,d, the spectral features of the (M@M)* and (S@M)* DWCNTs (dashed lines) are broad, and a large scattering background is observed. This is an indication of bundles[19], the presence of metallic catalysts[20], or other carbonaceous impurities[16] within the suspension. The extended centrifugation conditions are capable of pelleting these species, and the resulting M@M and S@M fractions contained only individualized DWCNTs. This was confirmed by atomic force microscopy (AFM) and scanning electron microscopy (SEM) images, as shown in Supplementary Fig. 4, where significantly larger bundles and aggregates can be seen in the (M@M)* and (S@M)* fractions than after centrifugation. It is unclear why the metallic outer-wall DWCNTs contain more bundles and impurities than their semiconducting counterparts, but this is in agreement with previous work by Moore and colleagues[12].

In M@M, only M_{11}^{inner} and M_{11}^{outer} peaks can be seen as a broad peak between 600 and 900 nm, and in the S@M sample, two clear peaks associated with M_{11}^{outer} at 850 nm and S_{11}^{inner} at 1,200 nm can be seen. An S_{11}^{outer} can be seen neither in the M@M case nor the S@M case, highlighting the high selectivity for metallic outer walls. However, it should be mentioned that a small contribution of M_{11}^{inner} can be seen in the S@M fraction at 650 nm. For the metallic outer-wall DWCNTs, the position of M_{11}^{outer} is similar and indicates a diameter of 1.6–2.1 nm, making them slightly larger than their semiconducting counterparts. To provide an indication of the nanotube concentration at each step, Supplementary Fig. 5 shows un-normalized absorption spectra for each of the DWCNT types at the various stages of processing, while the photograph in Fig. 4a shows the colour of the four different fractions.

Within the field of carbon-nanotube separation, Raman spectroscopy has routinely been used to characterize CNT dispersions[21–23] and it is now applied to the DWCNT fractions. Traditionally, the quality of carbon-nanotube separations has been characterized by single line excitation Raman spectroscopy[10,13], and this can be seen in Supplementary Fig. 6a for excitation wavelengths of 532, 633 and 785 nm. A Kataura plot[15] is provided in Supplementary Fig. 6b to aid interpretation. For DWCNTs, the interpretation of Raman spectroscopy is complicated, and the position of well-known SWCNT radial breathing modes (RBMs) cannot simply be mapped onto the different wall types of a DWCNT. Hirschmann *et al.*[24] have shown that the RBM position of SWCNTs is upshifted to 22.2 cm^{-1} on placing them within an

© 2017 Macmillan Publishers Limited, part of Springer Nature. All rights reserved.

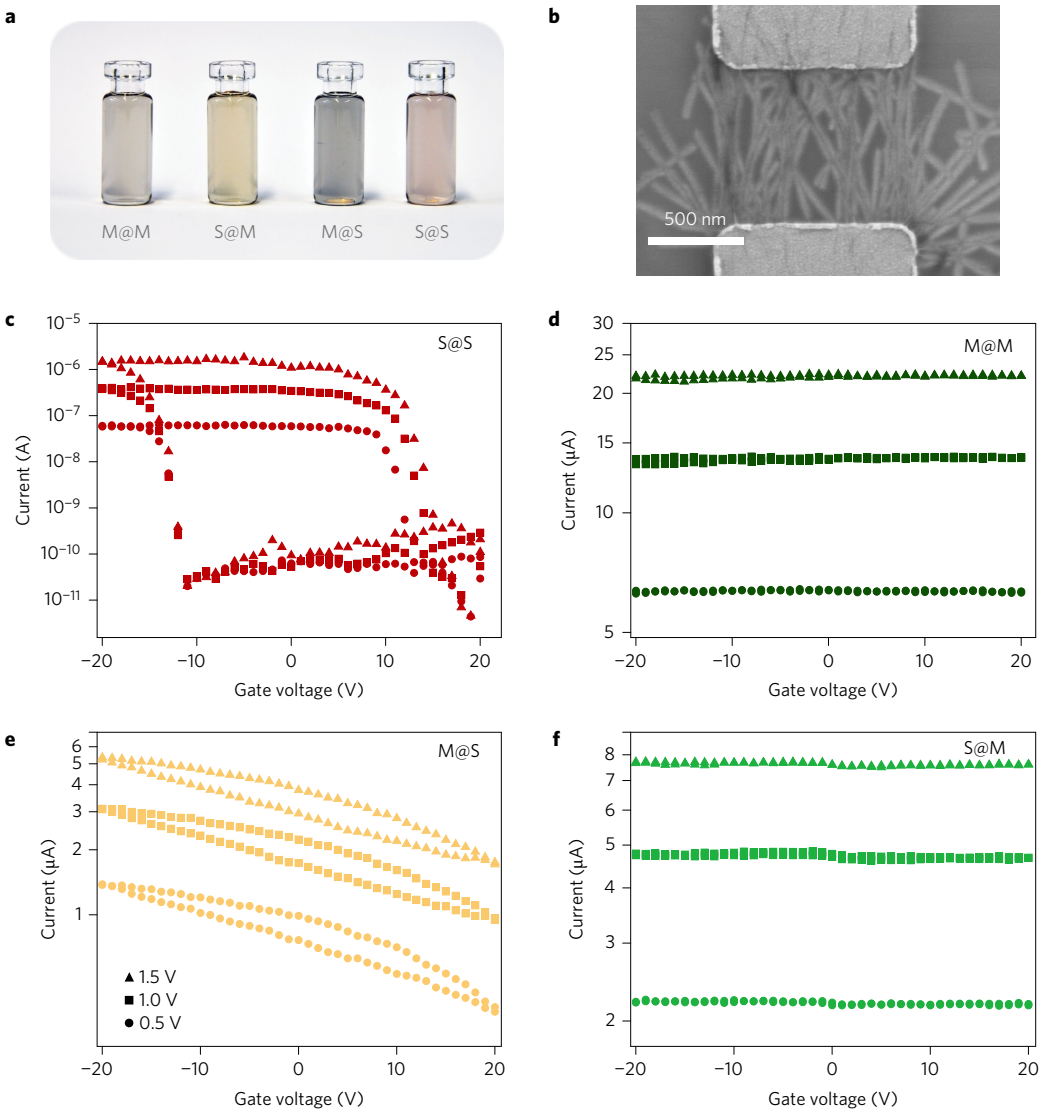

Figure 4 | Transconductance measurements of four types of DWCNT. a, Photograph of the purified DWCNT fractions. **b**, SEM micrograph of S@S in a DWCNT-FET device with a density of 50–60 CNTs per μm between the palladium source and drain contacts spaced 800 nm apart. **c**–**f**, I_D–$V_G$$I_S$ curve of four types of DWCNT after purification with PFO-BPy at different source–drain voltages V_{SD}.

outer wall, and Liu *et al.*[7] have shown both red- and blueshifts, where the extent and type of shift is reliant on the inter-wall spacing.

To this end, resonance Raman maps are useful for the analysis of DWCNTs and are shown in Fig. 3. The maps are built from the RBM spectral region (125–350 cm^{-1}, $1/\omega_{RBM} \propto d_t$, where d_t is the carbon nanotube diameter), with RBM spectra obtained using 46 different excitation laser lines over the range 1.40–2.33 eV. Within this energy range, semiconducting (S_{22} at high RBM frequencies and S_{33} at low RBM frequencies) and metallic (M_{11} spanning lower and higher frequencies) optical transitions from different inner- and outer-wall nanotubes are resonantly excited. Although a spectral shift is expected for the constituent walls of a DWCNT compared to SWCNTs, analysis of RBM intensities within these maps delivers a clear picture of the nanotube population. The RBM frequencies and resonant energies of SWCNTs for all values of (n,m) in this range are shown in Supplementary Fig. 7 together with the excitation lines used to generate the maps. For the S@S and M@M fractions in Fig. 3a,b, respectively, interpretation is straightforward, with the clear presence of RBMs associated with S_{33}^{outer} and S_{22}^{inner} for S@S, and M_{11} (inner and outer) for M@M. The clear inner/outer splitting and the low degree of overlap between the data points of S@S and M@M indicate a high purity of the DWCNT fractions. The suppression of S_{33}^{outer} in Fig. 3b as compared to what is observed in the S@S map of Fig. 3a is a striking confirmation of the separation procedure. For M@S in Fig. 3c, analysis is also relatively simple, with the clear presence of S_{33}^{outer} and M_{11}^{inner}, and limited S_{22}^{inner}. Finally, when comparing Fig. 3c for M@S with the S@M in Fig. 3d, a suppression of S_{33}^{outer} and M_{11}^{inner} and an increase in S_{22}^{inner} are observed. In agreement with the absorption measurements in Fig. 2c,d, M@S and S@M contain a small fraction of semiconducting inner-wall and metallic inner-wall contamination, respectively.

For DWCNTs, an assessment of purity is difficult due to the overlapping inner- and outer-wall peaks and the inability to discriminate SWCNTs from the components of a DWCNT by optical absorption. For this reason, purity analysis by spectral fitting to first quantify the extent of SWCNT:DWCNT separation would be highly misleading, not to mention the classification by DWCNT electronic purity. On the other hand, transmission electron microscopy (TEM) can be used to confirm the presence of DWCNTs and the very small number of SWCNTs. Representative micrographs are shown in Supplementary Figs 8 and 9. Despite

© 2017 Macmillan Publishers Limited, part of Springer Nature. All rights reserved.

finding DWCNTs almost exclusively in each of the fractions, an analysis by TEM would also be misleading owing to the small number of nanotubes sampled and the inability to quickly discriminate between the four different types of DWCNT. In this regard it is only possible to look at spectral trends; both the resonance Raman maps and absorption measurements certainly suggest high electronic purity, but it remains difficult to quantify. In the resonance Raman maps shown in Supplementary Fig. 7 it can be seen that all species assigned to inner and outer walls do not line up with the expected RBM frequencies of SWCNTs. This suggests that all species have been perturbed by the presence of a second wall, and is strong spectroscopic evidence that the sample consists mostly of DWCNTs rather than a combination of SWCNTs. However, at this stage it remains highly complex to determine the (n,m) for individual pairs of inner and outer walls that might constitute a DWCNT.

High-density DWCNT FETs were built from both the (S@S)* and (S@S) fractions to help evaluate the electronic purity and demonstrate the role of the polymer in improving the semiconducting content. Transconductance measurements at source–drain voltages of 0.5, 1.0 and 1.5 V are presented in Supplementary Fig. 10a,b. For the (S@S)* sample, a single-order-of-magnitude on/off ratio, compared to that of the S@S device of approximately five orders of magnitude, clearly demonstrates the presence of small quantities of metallic species after gel separation. This is in agreement with the usual lower semiconducting purity of aqueous separations[25] and demonstrates the ability of the PFO–BPy to provide a final polishing and achieve electronics-grade S@S DWCNTs. In fact, due to the ability of aqueous sorting methods to prepare a large library of different (n,m) SWCNT species[26,27], the approach presented here for DWCNTs is likely to find application in improving the semiconducting purity of SWCNT fractions when an (n,m) selective polymer does not exist. DWCNT FETs were also prepared from M@M, M@S and S@M, and are shown in Fig. 4d–f for a high density of DWCNTs and in Supplementary Fig. 10e–g for a low density of DWCNTs. For each of the four different species a different transconductance curve is obtained, and its shape is invariant with increasing nanotube density. This suggests that a high level of electronic separation has been achieved and is further demonstrated statistically by a scatter plot from ~120 devices in Supplementary Fig. 10c. Most notable are the transconductance curves for S@M and M@S DWCNTs, because these differ from the purely metallic or semiconducting case. In agreement with previous measurements[9,12], S@M–FETs had an on/off ratio close to unity with a slight 'kink' in the source–drain current around $V_g = 0$ V, whereas M@S–FETs had only a slight modulation in source–drain current and an on/off ratio of ~1–2 orders of magnitude.

Conclusion

Despite the surfactant or polymer used for separation residing entirely on the outer wall, this work suggests that the two walls of a DWCNT are strongly coupled and that it is possible to develop a solution process sensitive to this interaction. In this work, the four different DWCNT types have been identified and separated. Gel chromatography was shown to be capable of enriching the different DWCNT types, and provided an exquisite example of the sensitivity of the surfactant shell to the electronic properties of a nanotube. Inter-wall coupling was similarly verified with the use of PFO–BPy in toluene, and residual metallic species were removed from the S@S fraction. Resonance Raman maps of sorted DWCNTs were measured, and contributions from the inner- and outer-wall species were identified and were found to be shifted relative to SWCNTs. Access to pure DWCNT samples will allow for the identification of a new set of RBMs associated with DWCNTs, and extended studies of the spectral shift induced upon placing one carbon wall within another will be possible. In particular it is expected that it will be possible to separate DWCNTs not only based on their inner- and outer-wall electronic type, but also based on chirality, and this will enable the investigation of single chirality species with different surrounding inner or outer walls. To achieve this it is proposed that DWCNTs must first be separated into the four electronic classes presented in this work and then separated by employing slight changes in solution pH or redox conditions. Central to the success of this approach will be the ability to perform a diameter-based fractionation of DWCNTs. In the current work and as shown in Supplementary Fig. 5e, a weak diameter fractionation is observed between fractions, but improving the resolution of this separation will now form the focus of future research.

Methods

Methods and any associated references are available in the online version of the paper.

Received 3 April 2017; accepted 5 September 2017;
published online 2 October 2017

References

1. Moore, K. E., Tune, D. D. & Flavel, B. S. Double-walled carbon nanotube processing. *Adv. Mater.* **27,** 3105–3137 (2015).
2. Okada, S. & Oshiyama, A. Curvature-induced metallization of double-walled semiconducting zigzag carbon nanotubes. *Phys. Rev. Lett.* **91,** 216801 (2003).
3. Zólyomi, V. *et al.* Semiconductor-to-metal transition of double walled carbon nanotubes induced by inter-shell interaction. *Phys. Status Solidi B* **243,** 3476–3479 (2006).
4. Kalbac, M., Green, A. A., Hersam, M. C. & Kavan, L. Probing charge transfer between shells of double-walled carbon nanotubes sorted by outer-wall electronic type. *Chem. Eur. J.* **17,** 9806–9815 (2011).
5. Shi, W. *et al.* Superconductivity in bundles of double-wall carbon nanotubes. *Sci. Rep.* **2,** 625 (2012).
6. Noffsinger, J. & Cohen, M. L. Electron–phonon coupling and superconductivity in double-walled carbon nanotubes. *Phys. Rev. B* **83,** 165420 (2011).
7. Liu, K. *et al.* Van der Waals-coupled electronic states in incommensurate double-walled carbon nanotubes. *Nat. Phys.* **10,** 737–742 (2014).
8. Zhang, R. *et al.* Superlubricity in centimetres-long double-walled carbon nanotubes under ambient conditions. *Nat. Nanotech.* **8,** 912–916 (2013).
9. Bouilly, D. *et al.* Wall-selective probing of double-walled carbon nanotubes using covalent functionalization. *ACS Nano* **5,** 4927–4934 (2011).
10. Green, A. A. & Hersam, M. C. Properties and application of double-walled carbon nanotubes sorted by outer-wall electronic type. *ACS Nano* **5,** 1459–1467 (2011).
11. Green, A. A. & Hersam, M. C. Processing and properties of highly enriched double-wall carbon nanotubes. *Nat. Nanotech.* **4,** 64–70 (2009).
12. Moore, K. E. *et al.* Sorting of double-walled carbon nanotubes according to their outer wall electronic type via a gel permeation method. *ACS Nano* **9,** 3849–3857 (2015).
13. Streit, J. *et al.* Separation of double-wall carbon nanotubes by electronic type and diameter. *Nanoscale* **9,** 2531–2540 (2017).
14. Hároz, E. H. *et al.* Fundamental optical processes in armchair carbon nanotubes. *Nanoscale* **5,** 1411–1439 (2013).
15. Weisman, R. B. & Bachilo, S. M. Dependence of optical transition energies on structure for single-walled carbon nanotubes in aqueous suspension: an empirical Kataura plot. *Nano Lett.* **3,** 1235–1238 (2003).
16. Flavel, B. S. *et al.* Separation of single-walled carbon nanotubes with a gel permeation chromatography system. *ACS Nano* **8,** 1817–1826 (2014).
17. Mistry, K. S., Larsen, B. A. & Blackburn, J. L. High-yield dispersions of large-diameter semiconducting single-walled carbon nanotubes with tunable narrow chirality distributions. *ACS Nano* **7,** 2231–2239 (2013).
18. Nish, A., Hwang, J.-Y., Doig, J. & Nicholas, R. J. Highly selective dispersion of single-walled carbon nanotubes using aromatic polymers. *Nat. Nanotech.* **2,** 640–646 (2007).
19. O'Connell, M. J. *et al.* Band gap fluorescence from individual single-walled carbon nanotubes. *Science* **297,** 593–596 (2002).
20. Chiang, I. *et al.* Purification and characterization of single-wall carbon nanotubes (SWNTs) obtained from the gas-phase decomposition of CO (HiPco process). *J. Phys. Chem. B* **105,** 8297–8301 (2001).
21. Maultzsch, J., Telg, H., Reich, S. & Thomsen, C. Radial breathing mode of single-walled carbon nanotubes: optical transition energies and chiral-index assignment. *Phys. Rev. B* **72,** 205438 (2005).
22. Araujo, P. T. *et al.* Third and fourth optical transitions in semiconducting carbon nanotubes. *Phys. Rev. Lett.* **98,** 067401 (2007).

© 2017 Macmillan Publishers Limited, part of Springer Nature. All rights reserved.

23. Pesce, P. *et al.* Calibrating the single-wall carbon nanotube resonance Raman intensity by high resolution transmission electron microscopy for a spectroscopy-based diameter distribution determination. *Appl. Phys. Lett.* **96,** 051910 (2010).
24. Hirschmann, T. C. *et al.* Role of intertube interactions in double- and triple-walled carbon nanotubes. *ACS Nano* **8,** 1330–1341 (2014).
25. Tulevski, G. S., Franklin, A. D. & Afzali, A. High purity isolation and quantification of semiconducting carbon nanotubes via column chromatography. *ACS Nano* **7,** 2971–2976 (2013).
26. Liu, H., Nishide, D., Tanaka, T. & Kataura, H. Large-scale single-chirality separation of single-wall carbon nanotubes by simple gel chromatography. *Nat. Commun.* **2,** 309 (2011).
27. Wei, X. J. *et al.* Experimental determination of excitonic band structures of single-walled carbon nanotubes using circular dichroism spectra. *Nature Commun.* **7,** 9 (2016).
28. Liu, K. *et al.* Quantum-coupled radial-breathing oscillations in double-walled carbon nanotubes. *Nat. Commun.* **4,** 1375 (2013).
29. Wang, H. *et al.* Solvent effects on polymer sorting of carbon nanotubes with applications in printed electronics. *Small* **11,** 126–133 (2015).

Acknowledgements

The authors acknowledge the experimental assistance of J. Zaumseil and S. Grimm and thank K. Moore and A. Blanch for discussions. B.S.F. acknowledges support from the Deutsche Forschungsgemeinschaft (DFG, under grants nos. FL 834/1-1 and FL 834/2-1). R. K. acknowledges funding by the DFG under INST 163/354-1 FUGG. R.K. and F.H. acknowledge support by the Helmholtz Association through the STN programme. G.G. and S.R. acknowledge the German Research Foundation (DFG, via SFB 658, subproject A6) and Focus Area NanoScale of the Freie Universität Berlin for financial support.

Author contributions

B.S.F., H.L. and F.H. devised and performed the DWCNT separation. G.G., S.W., A.J., R.K., S.R., H.L. and B.S.F. performed and analysed the resonance Raman maps. TEM measurements were performed by V.S.K.C., S.K.C.N., H.L. and B.S.F. All authors contributed to the preparation of the final manuscript.

Additional information

Supplementary information is available in the online version of the paper. Reprints and permissions information is available online at www.nature.com/reprints. Publisher's note: Springer Nature remains neutral with regard to jurisdictional claims in published maps and institutional affiliations. Correspondence and requests for materials should be addressed to H.L. and B.S.F.

Competing financial interests

The authors declare no competing financial interests.

© 2017 Macmillan Publishers Limited, part of Springer Nature. All rights reserved.

Methods

Separation by gel permeation. DWCNTs (>60% DWCNT purity, lot no. DW27-096) with an average outer-wall diameter of ~2.0 nm were obtained from NanoIntegris. Raw powder (10 mg) was suspended in 20 ml of aqueous 1 wt% SC (Sigma-Aldrich) by tip sonication (Weber Ultrasonics, 35 kHz, 16 W in continuous mode) for 1 h. During sonication the suspension was cooled in a water bath at 5 °C. The resulting dispersion was centrifuged at 45,560*g* (Beckman Optima L-80 XP, SW 40 Ti rotor) for 1 h and the supernatant collected. NaOH was then added to 8 ml of the DWCNT dispersion to obtain the 'start material' for gel separation with NaOH concentrations of 0, 1 and 4 mM. Gel permeation chromatography was performed as previously described[12,16], using the Sephacryl S-200 gel medium (GE Healthcare) in a glass column (45 cm in length with a 2 cm inner diameter). Before the addition of DWCNTs, the column was washed with 150 ml of 1 wt% SDS (Merck KGaA) containing a NaOH concentration corresponding to the DWCNT 'start material'. Following the addition of DWCNTs a 1 wt% SDS solution was used as the eluent and a constant flow rate of 2 ml min^{-1} was maintained by N_2 overpressure. Fractions (3 ml) were collected from the column and any adsorbed species were finally eluted by addition of 1 wt% SC without NaOH. Throughout elution, a Raman RXN Systems Analyzer (Kaiser Optical Systems) with an excitation wavelength of 785 nm was used to monitor the integrated G-mode intensity. Fractions containing separated DWCNTs from gel permeation were labelled (M@M)*, (S@M)*, (M@S)* and (S@S)*.

Purification by polymer wrapping. The four gel-separated DWCNT fractions were filtered onto 0.45 μm Nylon membranes (Phenomenex), washed repeatedly with water and acetone to remove any surfactants and dried overnight in an oven at 120 °C. The dry filter cake was then resuspended by sonication for 1 h with 1 mg ml^{-1} poly[(9,9-dioctylfluorenyl-2,7-diyl)-alt-co-(6,6′-{2,2′-bipyridine})] (PFO–BPy) (American Dye Source) in two different organic solvents: metallic outer wall enriched fractions, (M@M)* and (S@M)*, in chlorobenzene and the semiconducting outer wall fractions, (M@S)* and (S@S)*, in toluene. Chlorobenzene was chosen as it has a higher polarizability than toluene, a higher density than THF[29], and has been shown to lead to a reduced semiconducting selectivity of polymer wrapping agents[29]. The (M@M)* and (S@M)* samples were centrifuged at 71,700*g* for 12 h (Beckman Optima MAX-E, TLA-55 rotor) and the top 80% of the supernatant collected as purified M@M and S@M. The (M@S)* and (S@S)* samples in toluene were centrifuged at 17,900*g* for 1 h. For the (S@S)* sample the top 80% of the supernatant was collected as purified S@S. For the (M@S)* sample the supernatant was discarded and the pellet resuspended in 1 mg ml^{-1} PFO-BPy toluene solution by sonication. This process was repeated approximately five times or until the absorption measurement of the supernatant started showing M_{11} peaks from inner-wall CNTs. The final pellet was dried and resuspended in *o*-xylene to yield the purified M@S sample.

Optical characterization. Absorption spectra were recorded on a Varian Cary 500 spectrophotometer and no background subtraction was used. Raman absorption spectra were taken with an InVia-Reflex confocal Raman microscope (Renishaw) with laser energies of 1.58 eV (785 nm), 1.96 eV (633 nm) and 2.33 eV (532 nm) under a ×50 objective. Power and gratings were optimized appropriately for each excitation wavelength. Resonant Raman maps of sorted DWCNT material were measured on pelleted samples. All samples were centrifuged (Optima Max-XP) at 100,000*g* for 1 h and dispersed onto a silicon substrate. The S@M DWCNTs were additionally centrifuged for an additional hour at 200,000*g*. Raman spectra were measured at the same position on the sample with a tunable laser system. A fluorescent dye laser (Radiant Dyes) with different dyes (R6G: 560–615 nm and DCM: 620–670 nm) and a Coherent Ti:sapphire laser (690–885 nm) were used. The laser power was kept constant at 500 μW to avoid heating the sample. The Raman response of the nanotubes was corrected to a CaF_2 reference. The laser light was guided through a ×100 microscope objective and measured with a T64000 Horiba Jobin Yvon spectrometer with a silicon charge-coupled device (CCD) in backscattering configuration. The spectra were normalized at ~1.3 nm, as indicated by a dashed line in the resonance Raman maps.

SEM and AFM measurement. A Zeiss Ultra Plus with 2.00 kV EHT, 2.9 mm working distance, and a magnification of 50,000 was used for SEM imaging. AFM measurements were acquired with a Bruker Dimension FastScan with NanoScope V controller, NanoScope control software (version 8.15) and ScanAsyst Air cantilevers. The peak-force tapping imaging mode was used with the scan rate and set point controlled manually, while the feedback gains and Z-limit were automatically adjusted to optimize image quality.

FET device fabrication. CNT–FET devices were fabricated on p-doped silicon (0.005–0.001 Ω cm, 325 μm thickness, CZ, ⟨100⟩, ABC) with an 800 nm thermally grown oxide as the gate dielectric. Palladium source and drain electrodes with a spacing of 800 nm were fabricated by electron-beam lithography, metal sputtering and liftoff. To deposit nanotubes, 50 μl of a dispersion was placed on top of the substrate and an electric field of 4 V was applied between the source and drain electrodes for 5 min. The substrate was rinsed ten times with toluene before drying with nitrogen. Electronic measurements were obtained with an Agilent 4155C semiconductor parameter analyser.

TEM measurement. TEM samples were prepared by drop-casting aqueous suspensions of the nanotubes onto lacy carbon-coated copper grids (Quantifoil). Subsequently, samples were washed with toluene and dried. TEM analysis was performed using an aberration-corrected FEI Titan 80-300 microscope operated at 80 kV and equipped with a Gatan US1000 CCD camera for imaging and electron diffraction. All micrographs were obtained with a 2k × 2k CCD camera and analysed using the Digital Micrographs software package (Version 1.71.38, Gatan).

Data availability. The data that support the plots within this paper and other findings of this study are available from the corresponding author upon reasonable request.

© 2017 Macmillan Publishers Limited, part of Springer Nature. All rights reserved.